Functionalized Multilayered Graphene Platform for Urea Sensor

Rajesh K. Srivastava,[†,‡] Saurabh Srivastava,[†,§] Tharangattu N. Narayanan,[‡] Bansi D. Mahlotra,[§,⊥,∥] Robert Vajtai,[‡] Pulickel M. Ajayan,[‡] and Anchal Srivastava[†,*]

[†]Department of Physics, Banaras Hindu University, Varanasi, Uttar Pradesh 221005, India, [‡]Department of Mechanical Engineering and Material Science, Rice University, Houston, Texas 77005, United States, [§]Department of Science and Technology Centre on Biomolecular Electronics, Biomedical Instrumentation Section, National Physical Laboratory, New Delhi 110012, India, [⊥]Centre for NanoBioengineering & Spin Tronics, Chungnam National University, 220 Gung-Dong Yuseong-Gu, Daejeon 305-764, Korea, and [∥]Department of Biotechnology, Delhi Technological University, Delhi 11042, India

ABSTRACT

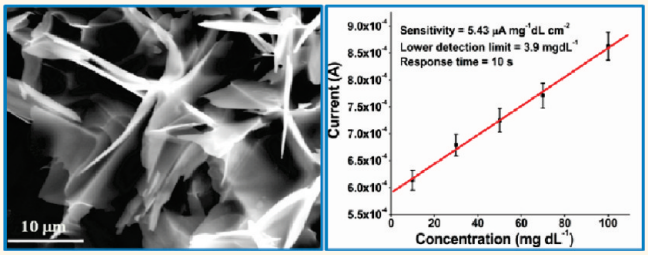

Multilayered graphene (MLG) is an interesting material for electrochemical sensing and biosensing because of its very large 2D electrical conductivity and large surface area. We propose a less toxic, reproducible, and easy method for producing functionalized multilayer graphene from multiwalled carbon nanotubes (MWCNTs) in mass scale using only concentrated H_2SO_4/HNO_3. Electron microscopy results show the MLG formation, whereas FTIR and XPS data suggest its carboxylic and hydroxyl-functionalized nature. We utilize this functionalized MLG for the fabrication of a novel amperometric urea biosensor. This biosensor shows linearity of 10—100 mg dL^{-1}, sensitivity of 5.43 μA mg^{-1} dL cm^{-2}, lower detection limit of 3.9 mg dL^{-1}, and response time of 10 s. Our results suggest that MLG is a promising material for electrochemical biosensing applications.

KEYWORDS: MWCNTs · graphene · biosensor · electron microscopy · X-ray photoelectron spectroscopy

In recent years, graphene has become an exciting material for research due to its fascinating physical properties, such as quantum electron transport,[1,2] a tunable band gap,[3] high carrier mobility,[1,2,4,5] high elastic behavior,[6] and excellent electrochemical properties[7] that make it a promising material for nanobioelectronic devices.[8−10] Graphene is a flat monolayer of carbon atoms, tightly packed into a two-dimensional (2D) honeycomb lattice. Realizing potential applications of graphene, an easy and less toxic method for preparation at large scale, is urgently needed. The very first time, in 1958, Hummers reported the synthesis of graphite oxide using $KMnO_4$ and $NaNO_3$ in concentrated H_2SO_4,[11] but this method involves many tedious steps and requires explosive chemicals which generate highly toxic gases such as NO_2 and N_2O_4. After this, a number of methods came into existence, including mechanical exfoliation,[4] chemical vapor deposition (CVD),[5] plasma etching,[12] solvothermal synthesis,[13] and chemical route[14−16] for the formation of graphene and reduced graphene oxide. Among these, CVD is a useful method to grow large and highly ordered single and multilayered graphene, but the large-scale production continues to be a challenge. Moreover, it requires very high temperature as well as metallic substrate such as Ni, Cu, *etc.*,[17−21] which requires the transfer of graphene on insulating substrates to measure its transport properties. There is thus a need to develop an easy synthesis route that can be used for large-scale production without using any substrates. Recently, CNTs (both SWNTs and MWCNTs) have been explored for making different layers of graphene with varying lengths from a few nanometers to micrometer range using oxidizing chemical routes[22,23] and plasma etching.[12]

The functionalized graphene has been used for various applications mainly in gas sensors,[24] chemical sensors,[25] biosensors,[7,26] supercapacitors,[27] batteries,[28] *etc.* and in the formation of a nanocomposite with polymers/nanoparticles.[29−31]

We report a simple and reproducible method for large-scale production of functionalized multilayer graphene (MLG) from MWCNTs by the chemical method using oxidizing agents, namely, concentrated H_2SO_4 and HNO_3, that help in unzipping of MWCNTs. Extensive experimental studies with different time intervals and with different concentrations of these reagents have been performed to obtain the optimum condition that provides

* Address correspondence to anchalbhu@gmail.com.

Received for review August 20, 2011 and accepted November 27, 2011.

Published online November 27, 2011
10.1021/nn203210s

an easy and large-scale production of MLG. Since functionalized graphene has a large surface area, extraordinary electronic transport behavior, good biocompatibility, and a carboxylic functional group that makes it a useful material for biosensing and electrochemical applications.[7,32,33] Since most atoms of the graphene sheets are exposed to the surface, slight changes in the charge environment due to the adsorption of biomolecules provide significant changes in their electrical properties which help in fabrication of more sensitive sensors.[34] Moreover, graphene does not contain the catalytic impurities such as Fe, Ni, *etc.*[35] that are mostly present in carbon nanotubes, and thus it reduces interference caused by these impurities and offers more reproducible sensing response.[36−39]

Keeping the above in view, we have explored this functionalized MLG for a novel urea biosensing application employing an electrochemical technique. Urea is an important analyte of clinical interest (normal level in blood 15−40 mg/dL), its early detection can be helpful to prevent various kidney diseases like renal failure, urinary tract obstruction, hepatic failure, and nephritic syndrome.[40] Here, a thin film of functionalized MLG has been fabricated onto an indium tin oxide (ITO) substrate by electrophoretic deposition (EPD) technique and has been used to immobilize urease and glutamate dehydrogenase (GLDH) using ethyl(dimethylaminopropyl)carbodiimide and *N*-hydroxysuccinimide (EDC-NHS) chemistry for the development of a novel amperometric urea biosensor.

RESULTS AND DISCUSSION

Morphological Characterizations of MLG. Scanning electron microscopy (SEM) has been done to characterize surface morphology of MLG taken over the Si/SiO_2 substrate. Figure 1a−f shows SEM micrographs at different time intervals during the conversion process of MWCNTs into MLG. After 6 h sonication of MWCNTs under H_2SO_4/HNO_3 oxidizing agent, there is no significant change observed in the surface structure of MWCNTs (Figure 1a). However, as we start vigorous stirring at 80 °C, MWCNTs begin to unzip in the graphene layer after a few minutes. So, we have tried to analyze the SEM of this sample stirred at different time intervals in Figure 1b−d. A sample collected after 20 min sonication is shown in Figure 1b. Figure 1b exhibits evidence for the initiation of the unzipping process and formation of MLG. It can be seen that some of the MWCNTs are still present, as shown by the arrows. A similar feature is observed in the sample collected after 25 min (Figure 1c), with the only difference being that the concentration of MWCNTs is reduced and most of the nanotubes have been converted into MLG. Figure 1d−f represents micrographs after quenching the ongoing reaction for 30 min followed by filtering and washing until neutral pH = 7.0 is reached. It gives clear evidence of the conversion of all of the MWCNTs into MLG. It seems

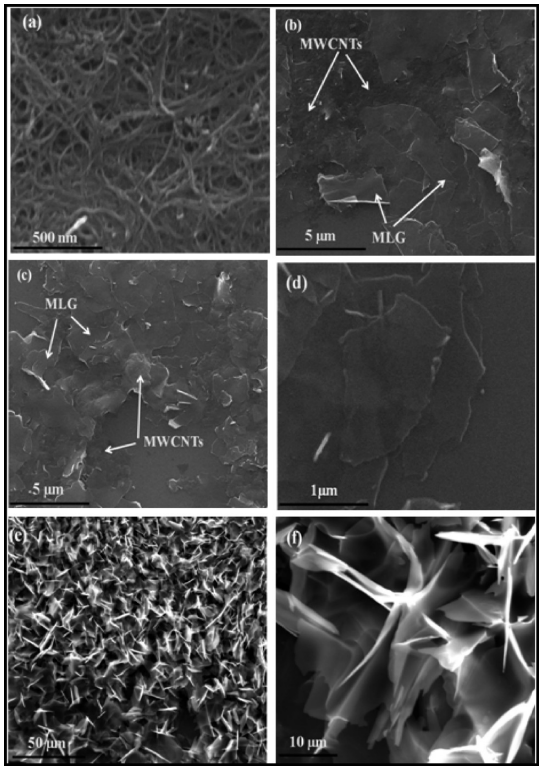

Figure 1. SEM micrograph at different time intervals during the conversion process of MWCNTs into MLG. It gives evidence for the conversion of all of the MWCNTs into a graphene layer during acid oxidation treatment (a−f). (a) Sonicated MWCNTs after 6 h at 50 kHz. (b,c) Micrographs at different stirring times, which confirms the formation of MLG, and (d−f) where all of the MWCNTs have been converted into MLG.

that the individual graphene flakes stack together to form larger size platelets when we quenched the reaction after 30 min (see Supporting Information Figure S1).

Figure 2 shows the transmission electron microscopic (TEM, panels a−d) and selected area electron diffraction (SAED, panel e) pattern of MLG, which suggests the formation of MLG through unzipping of MWCNTs by action of the H_2SO_4/HNO_3, where MWCNTs have an outer diameter ranging from 20 to 40 nm. Most of the micrographs in Figure 2a are found to be MLG (indicated by the arrows). The synthesized graphene sheets show a tendency to stack into overlapped layers. It can be seen from TEM analysis that resulting graphene sheets not only show tendency to stack layers but also tend to form larger graphene sheets derived from aggregation of a few graphene layers. The brighter area in Figure 2a corresponds to a thinner layer graphene, whereas the darker area is made up of thicker layers. Figure 2b−d represents the high-resolution TEM micrograph from a different region of MLG, where the graphitic planes are clearly visible. Figure 2e represents the SAED pattern of MLG. This SAED pattern indicates the hexagonal atomic structure and crystalline nature of the flakes. It shows six sets of hexagonal spots with a rotational angle around 6, 8, and 11° between different sets of layers.

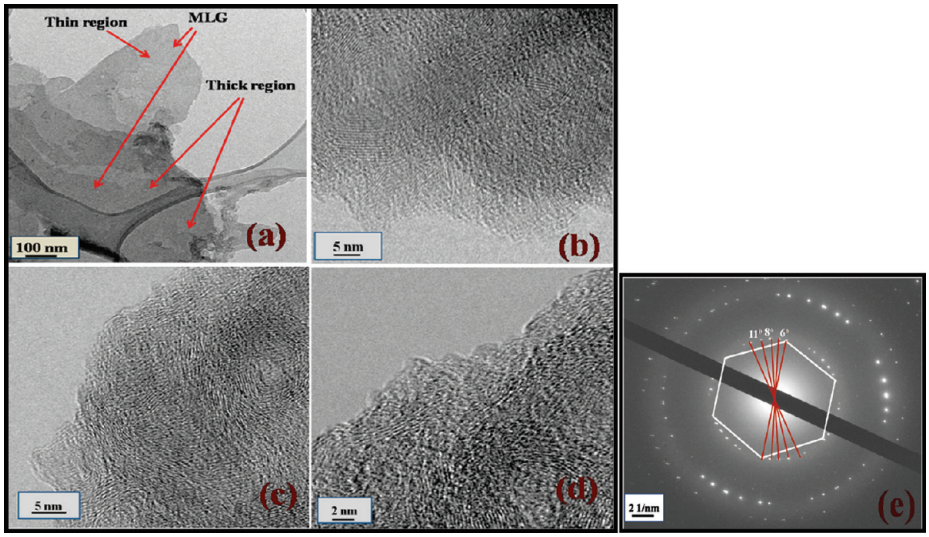

Figure 2. TEM image of functionalized MLG. (a) Thick and thin region of MLG has been observed. (b–d) HRTEM images of MLG, where the graphitic planes are clearly visible. (e) SAED of MLG, which confirms the hexagonal atomic structure and crystalline nature of the flakes.

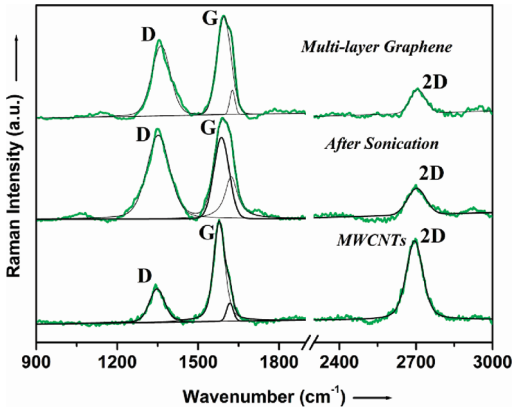

Figure 3. Raman spectra of pristine MWCNTs, after sonication and functionalized MLG. In this, D, G (G_1 and G_2), and 2D Raman bands of MWCNTs, MWCNTs after sonication, and MLG have been fitted using SpectraCalc software.

The six-layer stackings have also been confirmed by XRD analysis (see Supporting Information Figure S2). The rotational disorder is evident from the SAED pattern (Figure 2e), which indicates that the flakes are randomly oriented.[41]

AFM is a sensitive and flexible technique which is used for measurement of the thickness of MLG. The MLG suspension in dimethyl fluoride (DMF) is spin-coated (5000 rpm) onto the Si/SiO_2 substrate followed by drying at room temperature, and it has been used for AFM analysis. The image and detailed explanation is shown in Supporting Information, Figure S3.

Structural Characterizations of MLG. Raman spectroscopy is a powerful tool to investigate the structural aspects of carbon-based materials. In this study, the Raman spectrum has been recorded for all of the samples by exciting the samples with an excitation wavelength of 514.5 nm. Figure 3 represents the Raman spectrum of MWCNTs, MWCNTs after 6 h of sonication, and the functionalized MLG. In order to observe the peak position and full width of half-maxima (fwhm) of D, G, and 2D Raman bands of MWCNTs, MWCNTs after sonication, and MLG, these bands have been fitted using SpectraCalc software. The calculated peak positions along with the fwhm of all observed bands (D, G_1, G_2, and 2D) for MWCNTs, MWCNTs after sonication, and MLG are shown in Table 1. In the spectrum (Figure 3), experimental data curve is shown in green, whereas the fitted curves are shown in black. The Raman spectra of pristine MWCNTs reveal the D band at 1342 cm^{-1} (due to disorder), the G band at 1580 cm^{-1} (because of graphitic nature), and the 2D band at 2698 cm^{-1} (second order of D band).[42,43] The 2D peak detected in the Raman spectra of all carbonaceous materials, which is essentially the second harmonic of the D band, comes out at $\sim 2\omega_D$ wavenumber position, when sp^2-bonded carbon atoms are present.[42,44] This 2D peak reveals a strong dispersive character as a function of excitation energy. The G band splitting into G_1 and G_2 can be seen for all samples. This splitting in MWCNTs is due to a change in the curvature of inner and outer cylinder tubes of MWCNTs,[45] whereas splitting of the G band in functionalized MLG perhaps occurs due to the presence of functional groups, which may change the curvature of

TABLE 1. Peak Position and Full Width of Half Maxima (fwhm) of D, G (G_1 and G_2), and 2D Raman Bands of MWCNTs, MWCNTs after Sonication, and MLG

	peak position (cm^{-1})			fwhm (cm^{-1})		
band	MWCNTs	after sonication	MLG	MWCNTs	after sonication	MLG
D	1347.5	1352.2	1362.2	67.5	102.1	82.9
G_1	1578.1	1586.4	1595.6	50.1	68.2	62.7
G_2	1617.8	1622.6	1626.9	30.2	55.7	23.1
2D	2694.2	2702.3	2707.2	78.5	86.5	72.0

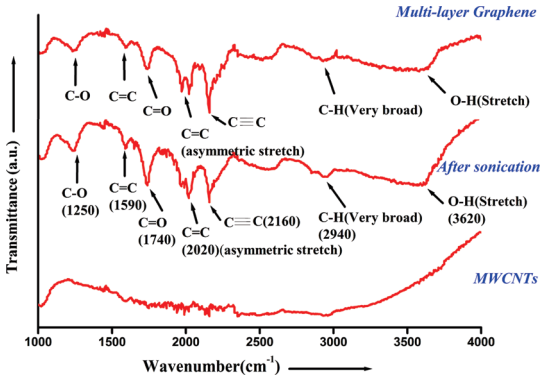

Figure 4. FTIR spectrum of MWCNTs, sonicated MWCNTs, and functionalized MLG. FTIR spectra reveal that both sonicated MWCNTs and MLG have carboxyl functional groups.

graphene layers. The attachment of functional group introduces sp^3 character in MLG. The different peaks positions (*i.e.*, D, G_1, G_2, and 2D) of MWCNTs after sonication and of MLG depict a shift at higher wavenumber compared to MWCNTs, which is shown in Table 1. The changes in the crystallinity analyzed by comparing the calculated fwhm values of all the bands are observed in the spectrum. The fwhm of the D band for MWCNTs is found to be ~67.5 cm^{-1}, whereas the fwhm for MWCNTs after sonication and MLG was enhanced up to 102.1 and 82.9 cm^{-1}, respectively. This enhancement shows the disordered behavior of MLG due to the attachment of functional groups as compared to MWNCTs. The fwhm of the G_1 and G_2 bands for MWCNTs are 50.1 and 30.2 cm^{-1}, respectively, whereas MWCNTs after sonication and MLG show that the fwhm of G_1 and G_2 are 68.2 and 55.7 cm^{-1} and 62.7 and 23.1 cm^{-1}, respectively. The fwhm of the 2D band for MWCNTs is around 78.5 cm^{-1}, whereas the fwhm after sonicated and MLG are at 86.5 and 72.0 cm^{-1}, respectively.

Figure 4 shows the FTIR spectra of MWCNTs, sonicated MWCNTs, and functionalized MLG. It can clearly be seen that both sonicated MWCNTs and MLG have more hydrophilic functional groups at the edge and on the surfaces. However, none of these peaks are seen in the case of MWCNTs, which exhibit the hydrophobic nature of the functional groups. The peak at 1740 cm^{-1} represents the stretching vibration of C═O bonds of the carboxylic acid group, whereas two other peaks at 2940 and 3620 cm^{-1} correspond to C−H and O−H stretching modes of the carboxylic alcohol groups, respectively. The peaks seen at 1250 and 1590 cm^{-1} represent the C═O and C═C stretching modes of MLG. FTIR spectra, thus, clearly suggest that −COOH groups are present within the MLG, which makes it a potential material for different applications. There are two additional peaks such as C═C (asymmetric stretch) and C═C observed at 2020 and 2160 cm^{-1}, respectively.

XPS is a quantitative spectroscopic technique that measures the elemental composition of the elements

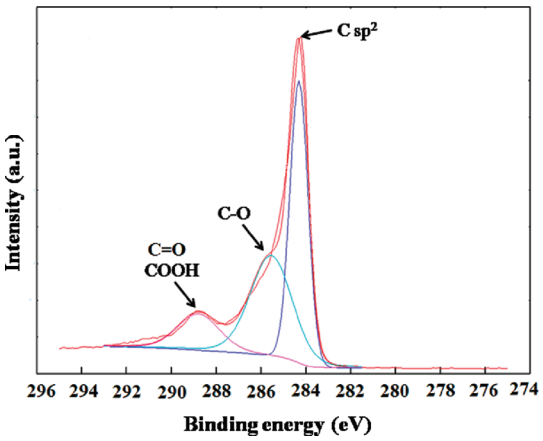

Figure 5. XPS study of functionalized MLG. In the XPS spectra, the peak at 284.2 eV is attributed to the presence of a graphitic structure (C═C), whereas the peak at 288.9 eV is assigned to the carbon 1s of the carboxylic group containing C═O.

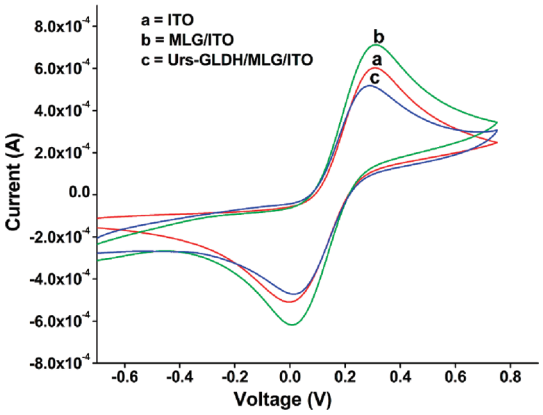

Figure 6. Cyclic voltammetry (CV) of ITO electrode (curve a), MLG/ITO electrode (curve b), and Urs-GLDH/MLG/ITO bioelectrode (curve c). The increase in the anodic current obtained for the MLG/ITO (0.71 mA, curve b) compared to bare ITO electrode (0.6 mA, curve a) indicates that a larger surface area of MLG helps in large-scale redox conversion.

that exists within a material which gives complete information about the surface chemistry of a material. Figure 5 represents XPS studies of carbon 1s spectra of the functionalized MLG, and it is deconvoluted into three species using Multipack software, version 7.0. In the XPS spectra of the graphene layer, a peak obtained at 284.2 eV is attributed to the presence of a graphitic structure (C═C) .The peak obtained at 288.9 eV is assigned to the carbon 1s of the carboxylic group (C═O). A relatively small intensity peak seen at 285.9 eV is due to the presence of a C−O bond.[46] Therefore, both XPS and FTIR studies confirm the formation of functionalized graphene.

Electrochemical Characterization. MLG/ITO electrode and Urs-GLDH/MLG/ITO bioelectrode have been characterized using the cyclic voltammery (CV) technique using Autolab, a potentiostat/galvanostat (Eco Chemie, Netherlands) with a three-electrode system in phosphate buffer (PBS) containing 5 mM $\{[Fe(CN)_6]^{3-/4-}$.

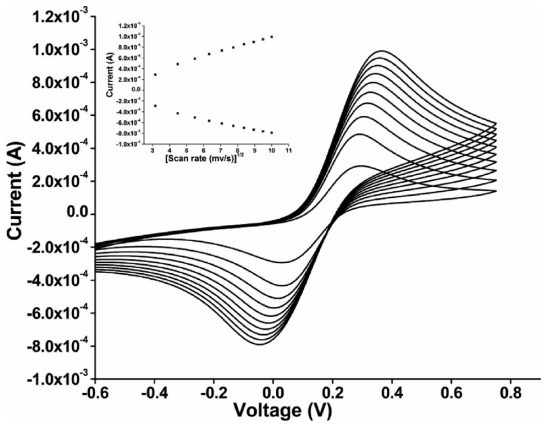

Figure 7. Cyclic voltammerty (CV) studies of the Urs-GLDH/MLG/ITO bioelectrode as a function of scan rate (10−100 mV/s). Inset: redox peak current of Urs-GLDH/MLG/ITO bioelectrodes as a function of the square root of scan rate. This result represents that, as we move toward a higher scan rate, anodic potential shifts more toward the positive potential and the cathodic peak potential shifts in the reverse direction.

Figure 6 shows the CV response obtained for ITO, MLG/ITO, and Urs-GLDH/MLG/ITO electrodes in the potential range of −0.75 to 0.75 V at a scan rate of 30 mV/s. The increase in the cathodic current obtained for the MLG/ITO (0.71 mA, curve b) compared to bare ITO electrode (0.6 mA, curve a) indicates that a larger surface area of MLG helps in large-scale redox conversion, resulting in an increase in the redox current which also reflects its enhanced electron transfer property. The decrease in the anodic current obtained for the Urs-GLDH/MLG/ITO electrode (0.52 mA, curve c) is attributed to the hindrance caused by the macromolecular structure of enzymes indicating urease and GLDH immobilization.

Figure 7 shows the cyclic voltammogram (CV) of the Urs-GLDH/MLG/ITO electrode recorded at different scan rates (10−100 mV/s). It can be seen that, as we move toward a higher scan rate, anodic potential shifts more toward the positive potential and the cathodic peak potential shifts in the reverse direction. Besides this, the redox peak currents show linear behavior with the square root of the scan rate, $\nu^{1/2}$ (inset in Figure 7), revealing it as a diffusion-controlled electron-transfer process (eqs 1 and 2).

$$I_a(\text{Urs-GLDH/MLG/ITO})[\text{A}] = 2.21 \times 10^{-5}[\text{A}] + 9.92 \times 10^{-5}[\text{As/mV}] \times \{\text{scan rate(mV/s)}\}^{1/2} \quad (1)$$

$$I_c(\text{Urs-GLDH/MLG/ITO})[\text{A}] = -1.07 \times 10^{-4}[\text{A}] - 6.99 \times 10^{-5}[\text{As/mV}] \times \{\text{scan rate(mV/s)}\}^{1/2} \quad (2)$$

The diffusion coefficient value (D) of the redox species for the Urs-GLDH/MLG/ITO bioelectrode has been

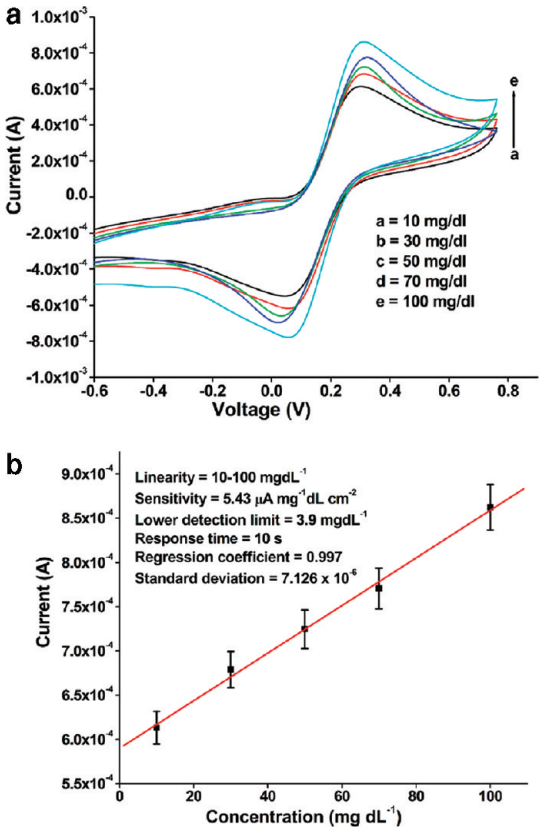

Figure 8. (a) CV response of the Urs-GLDH/MLG/ITO bioelectrode as a function of urea concentration in the presence of 30 μL of NADH and 70 μL of α-KG in PBS solution. (b) Calibration curve between magnitude of the anodic peak current (I_p) and urea concentration. It is found that the magnitude of the current increases linearly as urea concentration increases.

estimated from the slope of I_p *versus* $\nu^{1/2}$ plot using the Randel−Sevcik equation (eq 3)

$$I_p = (2.69 \times 10^5)n^{3/2}AD^{1/2}C\nu^{1/2} \quad (3)$$

where I_p is the peak current (I_{pa} anodic and I_{pc} cathodic), n is electron stoichiometry, A is electrode area (0.5 cm^2), D is diffusion coefficient, C is concentration of the redox species (5 mM $[Fe(CN)_6]^{3-/4-}$) in mol/cm^3, and ν is scan rate. The D value has been obtained as 2.65×10^{-8} cm^2 s^{-1}.

Electrochemical Response of the Urs-GLDH/MLG/ITO Bioelectrode. The responses of the Urs-GLDH/MLG/ITO bioelectrode have been studied by the CV method as a function of urea concentration. During the biochemical reaction, urease (Urs) catalyzes decomposition of urea into hydrogen bicarbonate (HCO_3^-) and ammonium (NH_4^+) ions. It has been found that ammonium ions simply diffuse into the solution. Thus it is required to add GLDH as it catalyzes the reaction among NH_4^+, α-KG, and NADH to create NAD^+ and L-glutamate. The electrons generated during the biochemical reactions are transferred to the electrode *via* an Fe(III)/Fe(IV) redox probe ensuing in a signal in the form of current.

TABLE 2. Sensing Characteristics of the Urs-GLDH/MLG/ITO Bioelectrode along with Those Reported in Literature

bioelectrode	detection range (linear) (mM)	detection limit (mM)	sensitivity	response time (s)	stability (days)	ref
Urs-GLDH/ZnO-Ch/ITO	0.8−16.6	0.49	0.13 μA/mM cm^{-2}	10	90	47
Urs/PAPCP/ITO	0.16−5.02		0.47 μA/mM cm^{-2}	40	60	48
Urs-PANi-nafion/Au	1−10	1	4.2 μA/mM cm^{-2}			49
Urs-SWCNT/glassy carbon	0.1−1 (nonlinear)	0.1		60		50
MWCNT/silica	2.18 × 10^{-2}−1.07		2.3 mV/mM cm^{-2}	25	60	51
Ur-GLDH/MLG/ITO	1.66−16.6	0.6474	32 μA/mM cm^{-2}	10	40	present work

The biochemical reaction is as follows:

$$(NH_2)_2CO + 3H_2O \xrightarrow{\text{urease}} 2NH_4^+ + OH^- + HCO_3^-$$

$$NH_4^+ + \alpha\text{-ketoglutarate} + NADH \xrightarrow{GLDH} \text{L-glutamate} + NAD^+$$

$$NADH \rightarrow NAD^+ + 2e^-$$

The electrochemical response studies of the Urs-GLDH/MLG/ITO bioelectrode obtained as a function of urea concentration in the presence of 30 μL of NADH and 70 μL of α-KG in PBS solution carried out using the CV technique has been shown in Figure 8a.

The calibration curve has been fitted between the urea concentration and the value of anodic peak current (Figure 8b). It is found that the magnitude of the current increases linearly as urea concentration increases (linear range as 10−100 mg/dL) and obeys eq 4 as below

$$I_p[A] = 5.899 \times 10^{-4}[A] + 2.691 \times 10^{-6}[A\,mg^{-1}\,dL] \times \{\text{urea concentration}(mg\,dL^{-1})\} \quad (4)$$

The Urs-GLDH/MLG/ITO bioelectrode exhibits linearity as 10−100 mg/dL, lower detection limit of 3.9 mg/dL, with the response time of 10 s. The sensitivity of the Urs-GLDH/MLG/ITO bioelectrode has been estimated as 5.43 μA mg^{-1} dL cm^{-2} with the regression coefficient of 0.997. The shelf life of the Urs-GLDH/MLG/ITO bioelectrode has been monitored by measuring electrochemical current response with respect to time, with a regular interval of 1 week. It is observed that this bioelectrode retains about 90% of the enzymes (Urs and GLDH) activity even after about 6 weeks when stored in refrigerated conditions (4 °C) after which the current response decreases to 85% in about 8 weeks. The effect of interferents on the Urs-GLDH/MLG/ITO bioelectrode has been evaluated by considering its CV response by adding normal concentration of interferents (data not shown) like cholesterol (5 mM), ascorbic acid (0.05 mM), uric acid (0.1 mM), and glucose (100 mg/dL) along with urea (1 mM) in phosphate buffer (50 mM, pH 7, 0.9% NaCl). The response remains nearly the same except for uric acid wherein there is an increase of about 7%. The sensing performance of the Urs-GLDH/MLG/ITO bioelectrode based urea biosensor is summarized in Table 2 along with those reported in the literature.

CONCLUSIONS

We have reported a new approach for large-scale production of functionalized MLG simply using concentrated H_2SO_4/HNO_3 from MWCNTs. SEM and HRTEM investigations have confirmed the synthesis of MLG, whereas FTIR and XPS have represented its functionalized behavior. This functionalized MLG has been successfully utilized in urea biosensor application employing an electrochemical technique, which suggests its potential application in electrochemical sensing and biosensing area. This biosensor shows linearity of 10−100 mg/dL, sensitivity of 5.43 μA mg^{-1} dL cm^{-2}, lower detection limit of 3.9 mg/dL, and response time of 10 s. The results of these studies have implications toward the application of this platform based on as synthesized graphene for estimation of other clinically important bioanalytes such as glucose, cholesterol, and triglycerides, *etc.*

EXPERIMENTAL DETAILS

Method of MWCNT Synthesis. MWCNTs have been synthesized by spray pyrolysis in a horizontal quartz tube furnace at ∼900 °C using xylene/ferrocene solution as a precursor. The optimum concentration of ferrocene in xylene used was 2 mg/mL. In this synthesis process, xylene is used as a carbon source, whereas Ar was used as a carrier gas at a flow rate of ∼300 sccm. The other experimental details have already been reported in our earlier reports.[52,53]

Formation of Functionalized MLG from MWCNTs. Prior to starting the graphene synthesis, MWCNTs are first treated with 5 M HCl to remove the catalytic impurities and amorphous carbon. After drying these purified MWCNTs in oven at 80 °C, it was used for chemical treatments. We have optimized the condition by varying different stirring time intervals and with different concentrations of these oxidizing agents which provide an easy and large-scale production of MLG. In the first step of synthesis, these purified MWCNTs are treated with concentrated H_2SO_4/HNO_3 (3:1) followed by ultrasonication at 50 kHz, and the samples are characterized at different time intervals. It has been observed that 6 h is the optimum time. In the second crucial step, solution is stirred vigorously at 80 °C. During the stirring process, the black color of the solution slowly turns brown in 15 min. This brown color is the evidence for the formation of graphene layers by unzipping MWCNTs. If we continue stirring at this stage, the brown color

turns yellow due to further breakage of graphene into very tiny size soluble graphene oxide. As soon as the brown color is observed, ongoing reaction is quenched by adding the distilled water or ice to restrict further reaction. The brown solution is filtered over a polytetrafluoroethylene (PTFE) membrane followed by washing several times with distilled water and finally dried at 80 °C overnight to get the desired MLG. In this synthesis process, the yield of MLG is found to be around 50% by weight of the starting material MWCNTs.

Fabrication of Functionalized MLG Thin Film Electrode. Thin film of nanostructured MLG over an ITO electrode is formed by electrophoretic deposition technique (EPD).[54] A very well dispersed stock solution of MLG (50 mg dL^{-1}) in acetonitrile is prepared by ultrasonication (50 W, 0.25 A) for about 1 h. Then, 100 μL of this stock solution is dispersed in 10 mL of acetonitrile to make the colloidal suspension of MLG. Its thin film is electrophoretically deposited using a two-electrode cell by applying a DC voltage. In order to get a surface charge on the MLG, 10^{-5}–10^{-4} mol of $Mg(NO_3)_2 \cdot 6H_2O$ is added into the suspension as electrolyte for EPD. A platinum foil (1 cm × 2 cm) is used as the cathode and a precleaned ITO-coated glass substrate having a sheet resistance of 30 Ω cm^{-1} as anode. The two electrodes, separated by 1 cm placed parallel to each other, are dipped in the MLG colloidal suspension. The film deposition is carried out onto the desired ITO-coated glass plate (0.5 cm^2) at 140 V for about 2 min. These films are then removed from the suspension followed by washing with deionized water and drying.

Covalent Immobilization of Urs and GLDH onto MLG/ITO Electrodes. All of the chemicals, namely, urease (Urs), glutamate dehydrogenase (GLDH), nicotinamide adenine dinucleotide (NADH), α-ketoglutarate (α-KG), *N*-hydroxysuccinimide (NHS), and ethyl-(dimethylaminopropyl)carbodiimide (EDC) have been procured from Sigma-Aldrich (USA). Urs (10 mg/mL) and GLDH (1 mg/dL) solutions are freshly prepared in phosphate buffer (50 mM, pH 7.0). The stock solution of urea (100 mg/dL) is prepared in deionized water and is kept at 4 °C. This stock solution is used to get different concentrations of urea by further dilution. EDC (100 mg/mL), NHS (20 mg/mL), NADH (3.7 mg/dL), and α-KG (47.5 mg/dL) are freshly prepared in doubly distilled water. Urs and GLDH were covalently attached to the MLG/ITO electrode by activating the COOH group of MLG using EDC as the coupling agent and NHS as activator.[55] The EDC-NHS-activated COOH group attached with a NH_2 terminal of Urs and GLDH results in the formation of a covalent amide bond (CO−NH). For COOH activation, the MLG/ ITO electrode is first dipped in PBS containing 0.4 M EDC and 0.1 M NHS for 4 h at room temperature. Further, 10 μL of bienzyme solution containing Urs (10 mg/mL) and GLDH (1 mg/mL) in 1:1 ratio has been immobilized by uniformly spreading on the activated electrode surface and kept for about 6 h. The Urs-GLDH/MLG/ITO bioelectrode is then washed with PBS buffer and is stored at 4 °C when not in use.

Acknowledgment. R.K.S. and S.S. acknowledges CSIR (SRF: 9/13(0170)/2008-EMRI) and CSIR (SRF: 31/001(0302)/2008-EMRI) New Delhi, India, for the financial support. A.S. acknowledges the DST, New Delhi, India, and CAS Department of Physics, Banaras Hindu University, India. We are very much thankful to Dr. Li. Song, Shinshu University, Japan, for helping in AFM analysis, and to Akshay Mathkar (graduate student), DMEMS, Rice University, Houston, Texas, for help in the FTIR measurements. The authors highly appreciate the help of Dr. Ana Laura Elia Arriaga, The Pennsylvania State University, for helping in SEM characterization. B.D.M. thanks the Ministry of Education, Science and Technology (R32-20026) of Korea for the opportunity for his visit to the Chungnam National University as visiting Professor during August 2011 under the World Class University Project.

Supporting Information Available: Schematic diagram of MLG formation. Detailed description of XRD pattern and AFM image. This material is available free of charge *via* the Internet at http://pubs.acs.org.

REFERENCES AND NOTES

1. Novoselov, K. S.; Geim, A. K.; Morozov, S. V.; Jiang, D.; Katsnelson, M. I.; Grigorieva, I. V.; Dubonos, S. V.; Firsov, A. A. Two-Dimensional Gas of Massless Dirac Fermions in Graphene. *Nature* **2005**, *438*, 197–200.
2. Zhang, Y.; Tan, Y.-W.; Stormer, H. L.; Kim, P. Experimental Observation of the Quantum Hall Effect and Berry's Phase in Graphene. *Nature* **2005**, *438*, 201–204.
3. Han, M. Y.; Oezyilmaz, B.; Zhang, Y.; Kim, P. Energy Band-Gap Engineering of Graphene Nanoribbons. *Phys. Rev. Lett.* **2007**, *98*, 206805.
4. Novoselov, K. S.; Geim, A. K.; Morozov, S. V.; Jiang, D.; Zhang, Y.; Dubonos, S. V.; Grigorieva, I. V.; Firsov, A. A. Electric Field Effect in Atomically Thin Carbon Films. *Science* **2004**, *306*, 666–669.
5. Berger, C.; Song, Z.; Li, X.; Wu, X.; Brown, N.; Naud, C.; Mayou, D.; Li, T.; Hass, J.; Marchenkov, A. N.; *et al.* Electronic Confinement and Coherence in Patterned Epitaxial Graphene. *Science* **2006**, *312*, 1191–1196.
6. Lee, C.; Wei, X.; Kysar, J. W.; Hone, J. Measurement of the Elastic Properties and Intrinsic Strength of Monolayer Graphene. *Science* **2008**, *321*, 385–388.
7. Pumera, M.; Ambrosi, A.; Bonanni, A.; Chng, E. L. K.; Poh, H. L. Graphene for Electrochemical Sensing and Biosensing. *Trends Anal. Chem.* **2010**, *29*, 954–965.
8. Castro Neto, A. H.; Guinea, F.; Peres, N. M. R.; Novoselov, K. S.; Geim, A. K. The Electronic Properties of Graphene. *Rev. Mod. Phys.* **2009**, *81*, 109.
9. Bunch, J. S.; Van der Zande, A. M.; Verbridge, S. S.; Frank, I. W.; Tanenbaum, D. M.; Parpia, J. M.; Craighead, H. G.; McEuen, P. L. Electromechanical Resonators from Graphene Sheets. *Science* **2007**, *315*, 490–493.
10. Westervelt, R. M. Graphene Nanoelectronics. *Science* **2008**, *320*, 324–325.
11. Hummers, W. S.; Offeman, R. E. Preparation of Graphitic Oxide. *J. Am. Chem. Soc.* **1958**, *80*, 1339–1339.
12. Jiao, L.; Zhang, L.; Wang, X.; Diankov, G.; Dai, H. Narrow Graphene Nanoribbons from Carbon Nanotubes. *Nature* **2009**, *458*, 877–880.
13. Choucair, M.; Thordarson, P.; Stride, J. A. Gram-Scale Production of Graphene Based on Solvothermal Synthesis and Sonication. *Nat. Nanotechnol.* **2009**, *4*, 30–33.
14. Schniepp, H. C.; Li, J.-L.; McAllister, M. J.; Sai, H.; Herrera-Alonso, M.; Adamson, D. H.; Prud'homme, R. K.; Car, R.; Saville, D. A.; Aksay, I. A. Functionalized Single Graphene Sheets Derived from Splitting Graphite Oxide. *J. Phys. Chem. B* **2006**, *110*, 8535–8539.
15. Rollings, E.; Gweon, G. H.; Zhou, S. Y.; Mun, B. S.; McChesney, J. L.; Hussain, B. S.; Fedorov, A. V.; First, P. N.; de Heer, W. A.; Lanzara, A. Synthesis and Characterization of Atomically Thin Graphite Films on a Silicon Carbide Substrate. *J. Phys. Chem. Solids* **2006**, *67*, 2172–2177.
16. Li, X.; Wang, X.; Zhang, L.; Lee, S.; Dai, H. Chemically Derived, Ultrasmooth Graphene Nanoribbon Semiconductors. *Science* **2008**, *319*, 1229–1232.
17. Shoushan, F.; Liang, L.; Ming, L. Monitoring the Growth of Carbon Nanotubes by Carbon Isotope Labelling. *Nanotechnology* **2003**, *14*, 1118.
18. Ferrari, A. C.; Meyer, J. C.; Scardaci, V.; Casiraghi, C.; Lazzeri, M.; Mauri, F.; Piscanec, S.; Jiang, D.; Novoselov, K. S.; Roth, S.; *et al.* Raman Spectrum of Graphene and Graphene Layers. *Phys. Rev. Lett.* **2006**, *97*, 187401.
19. Gilje, S.; Han, S.; Wang, M.; Wang, K. L.; Kaner, R. B. A Chemical Route to Graphene for Device Applications. *Nano Lett.* **2007**, *7*, 3394–3398.
20. Isett, L. C.; Blakely, J. M. Segregation Isosteres for Carbon at the (100) Surface of Nickel. *Surf. Sci.* **1976**, *58*, 397–414.
21. Srivastava, A.; Galande, C.; Ci, L.; Song, L.; Rai, C.; Jariwala, D.; Kelly, K. F.; Ajayan, P. M. Novel Liquid Precursor-Based Facile Synthesis of Large-Area Continuous, Single, and Few-Layer Graphene Films. *Chem. Mater.* **2010**, *22*, 3457–3461.
22. Kosynkin, D. V.; Higginbotham, A. L.; Sinitskii, A.; Lomeda, J. R.; Dimiev, A.; Price, B. K.; Tour, J. M. Longitudinal Unzipping of Carbon Nanotubes To Form Graphene Nanoribbons. *Nature* **2009**, *458*, 872–876.
23. Cano-Márquez, A. G.; Rodríguez-Macías, F. J.; Campos-Delgado, J.; Espinosa-González, C. G.; Tristán-López, F.; Ramírez-González, D.; Cullen, D. A.; Smith, D. J.; Terrones,

M.; Vega-Cantú, Y. I. Ex-MWNTs: Graphene Sheets and Ribbons Produced by Lithium Intercalation and Exfoliation of Carbon Nanotubes. *Nano Lett.* **2009**, *9*, 1527–1533.
24. Johnson, J. L.; Behnam, A.; Pearton, S. J.; Ural, A. Hydrogen Sensing Using Pd-Functionalized Multi-Layer Graphene Nanoribbon Networks. *Adv. Mater.* **2010**, *22*, 4877–4880.
25. Fowler, J. D.; Allen, M. J.; Tung, V. C.; Yang, Y.; Kaner, R. B.; Weiller, B. H. Practical Chemical Sensors from Chemically Derived Graphene. *ACS Nano* **2009**, *3*, 301–306.
26. Shao, Y.; Wang, J.; Wu, H.; Liu, J.; Aksay, I. A.; Lin, Y. Graphene Based Electrochemical Sensors and Biosensors: A Review. *Electroanalysis* **2010**, *22*, 1027–1036.
27. Yoo, J. J.; Balakrishnan, K.; Huang, J.; Meunier, V.; Sumpter, B. G.; Srivastava, A.; Conway, M.; Mohana Reddy, A. L.; Yu, J.; Vajtai, R.; *et al.* Ultrathin Planar Graphene Supercapacitors. *Nano Lett.* **2011**, *11*, 1423–1427.
28. Reddy, A. L. M.; Srivastava, A.; Gowda, S. R.; Gullapalli, H.; Dubey, M.; Ajayan, P. M. Synthesis of Nitrogen-Doped Graphene Films for Lithium Battery Application. *ACS Nano* **2010**, *4*, 6337–6342.
29. Gómez, H.; Ram, M. K.; Alvi, F.; Villalba, P.; Stefanakos, E.; Kumar, A. Graphene-Conducting Polymer Nanocomposite as Novel Electrode for Supercapacitors. *J. Power Sources* **2011**, *196*, 4102–4108.
30. Goswami, S.; Maiti, U. N.; Maiti, S.; Nandy, S.; Mitra, M. K.; Chattopadhyay, K. K. Preparation of Graphene–Polyaniline Composites by Simple Chemical Procedure and Its Improved Field Emission Properties. *Carbon* **2011**, *49*, 2245–2252.
31. Kamat, P. V. Graphene-Based Nanoarchitectures. Anchoring Semiconductor and Metal Nanoparticles on a Two-Dimensional Carbon Support. *J. Phys. Chem. Lett.* **2009**, *1*, 520–527.
32. Pumera, M. Electrochemistry of Graphene: New Horizons for Sensing and Energy Storage. *Chem. Rec.* **2009**, *9*, 211–223.
33. Liang, M.; Zhi, L. Graphene-Based Electrode Materials for Rechargeable Lithium Batteries. *J. Mater. Chem.* **2009**, *19*, 5871–5878.
34. Yang, W.; Ratinac, K. R.; Ringer, S. P.; Thordarson, P.; Gooding, J. J.; Braet, F. Carbon Nanomaterials in Biosensors: Should You Use Nanotubes or Graphene? *Angew. Chem., Int. Ed.* **2010**, *49*, 2114–2138.
35. Pumera, M. The Electrochemistry of Carbon Nanotubes: Fundamentals and Applications. *Chem.—Eur. J.* **2009**, *15*, 4970–4978.
36. Ambrosi, A.; Sasaki, T.; Pumera, M. Platelet Graphite Nanofibers for Electrochemical Sensing and Biosensing: The Influence of Graphene Sheet Orientation. *Chem. Asian J.* **2010**, *5*, 266–271.
37. Ambrosi, A.; Pumera, M. Stacked Graphene Nanofibers for Electrochemical Oxidation of DNA Bases. *Phys. Chem. Chem. Phys.* **2010**, *12*, 8943–8947.
38. Goh, M. S.; Pumera, M. The Electrochemical Response of Graphene Sheets Is Independent of the Number of Layers from a Single Graphene Sheet to Multilayer Stacked Graphene Platelets. *Chem. Asian J.* **2010**, *5*, 2355–2357.
39. Goh, M. S.; Pumera, M. Multilayer Graphene Nanoribbons Exhibit Larger Capacitance than Their Few-Layer and Single-Layer Graphene Counterparts. *Electrochem. Commun.* **2010**, *12*, 1375–1377.
40. Dhawan, G.; Sumana, G.; Malhotra, B. D. Recent Developments in Urea Biosensors. *Biochem. Eng. J.* **2009**, *44*, 42–52.
41. Ci, L.; Song, L.; Jin, C.; Jariwala, D.; Wu, D.; Li, Y.; Srivastava, A.; Wang, Z. F.; Storr, K.; Balicas, L.; Liu, F.; Ajayan, P. M. Atomic Layers of Hybridized Boron Nitride and Graphene Domains. *Nat. Mater.* **2010**, *9*, 430–435.
42. Heise, H. M.; Kuckuk, R.; Ojha, A. K.; Srivastava, A.; Srivastava, V.; Asthana, B. P. Characterisation of Carbonaceous Materials Using Raman Spectroscopy: A Comparison of Carbon Nanotube Filters, Single- and Multi-Walled Nanotubes, Graphitised Porous Carbon and Graphite. *J. Raman Spectrosc.* **2009**, *40*, 344–353.
43. Dresselhaus, M. S.; Dresselhaus, G.; Saito, R.; Jorio, A. Raman Spectroscopy of Carbon Nanotubes. *Phys. Rep.* **2005**, *409*, 47–99.
44. Heise, H. M.; Kuckuk, R.; Srivastava, A.; Asthana, B. P. Characterization of Carbon Nanotube Filters and Other Carbonaceous Materials by Raman Spectroscopy—II: Study on Dispersion and Disorder Parameters. *J. Raman Spectrosc.* **2011**, *42*, 294–302.
45. Zhao, X.; Ando, Y.; Qin, L.; Kataura, H.; Maniwa, Y.; Saito, R. Multiple Splitting of G-Band Modes from Individual Multi-walled Carbon Nanotubes. *Appl. Phys. Lett.* **2002**, *81*, 2550–2552.
46. Yang, D.; Velamakanni, A.; Bozoklu, G.; Park, S.; Stoller, M.; Piner, R. D.; Stankovich, S.; Jung, I.; Field, D. A.; Ventrice, C. A., Jr.; *et al.* Chemical Analysis of Graphene Oxide Films after Heat and Chemical Treatments by X-ray Photoelectron and Micro-Raman Spectroscopy. *Carbon* **2009**, *47*, 145–152.
47. Solanki, P. R.; Kaushik, A.; Ansari, A. A.; Sumana, G.; Malhotra, B. D. Zinc Oxide–Chitosan Nanobiocomposite for Urea Sensor. *Appl. Phys. Lett.* **2008**, *93*, 163903-3.
48. Rajesh; Bisht, V.; Takashima, W.; Kaneto, K. An Amperometric Urea Biosensor Based on Covalent Immobilization of Urease onto an Electrochemically Prepared Copolymer Poly(*N*-3-aminopropyl pyrrole-*co*-pyrrole) Film. *Biomaterials* **2005**, *26*, 3683–3690.
49. Luo, Y.-C.; Do, J.-S. Urea Biosensor Based on PANi(Urease)-Nafion®/Au Composite Electrode. *Biosens. Bioelectron.* **2004**, *20*, 15–23.
50. Xu, Z.; Chen, X.; Qu, X.; Jia, J.; Dong, S. Single-Wall Carbon Nanotube-Based Voltammetric Sensor and Biosensor. *Biosens. Bioelectron.* **2004**, *20*, 579–584.
51. Ahuja, T.; Kumar, D.; Singh, N.; Biradar, A. M.; Rajesh Potentiometric Urea Biosensor Based on Multi-Walled Carbon Nanotubes (MWCNTs)/Silica Composite Material. *Mater. Sci. Eng., C* **2011**, *31*, 90–94.
52. Awasthi, K.; Srivastava, A.; Srivastava, O. N. Synthesis of Carbon Nanotubes. *J. Nanosci. Nanotechnol.* **2005**, *5*, 1616–1636.
53. Srivastava, A.; Srivastava, O. N.; Talapatra, S.; Vajtai, R.; Ajayan, P. M. Carbon Nanotube Filters. *Nat. Mater.* **2004**, *3*, 610–614.
54. Dhand, C.; Singh, S. P.; Arya, S. K.; Datta, M.; Malhotra, B. D. Cholesterol Biosensor Based on Electrophoretically Deposited Conducting Polymer Film Derived from Nano-Structured Polyaniline Colloidal Suspension. *Anal. Chim. Acta* **2007**, *602*, 244–251.
55. Arya, S. K.; Solanki, P. R.; Datta, M.; Malhotra, B. D. Recent Advances in Self-Assembled Monolayers Based Biomolecular Electronic Devices. *Biosens. Bioelectron.* **2009**, *24*, 2810–2817.